NPT100-18A rescues mitochondrial oxidative stress and neuronal loss in human iPSC-based Parkinson's model

Julian E. Alecu
University Hospital Erlangen, Friedrich-Alexander University of Erlangen- Nürnberg
Veronika Sigutova
University Hospital Erlangen, Friedrich-Alexander University of Erlangen- Nürnberg
Razvan-Marius Brazdis
University Hospital Erlangen, Friedrich-Alexander University of Erlangen- Nürnberg
Sandra Lörentz
Friedrich-Alexander University of Erlangen- Nürnberg
Marios Bogionko
University Hospital Erlangen, Friedrich-Alexander University of Erlangen- Nürnberg
Anara Nursaitova
Friedrich-Alexander University of Erlangen- Nürnberg
Martin Regensburger
University Hospital Erlangen, Friedrich-Alexander University of Erlangen- Nürnberg
Laurent Roybon
Van Andel Institute
Kerstin M. Galler
University Hospital Erlangen, Friedrich-Alexander University of Erlangen- Nürnberg
Wolfgang Wrasidlo
Neuropore Therapies, Inc
Beate Winner
University Hospital Erlangen, Friedrich-Alexander University of Erlangen- Nürnberg
Iryna Prots
iryna.prots@uk-erlangen.de

University Hospital Erlangen, Friedrich-Alexander University of Erlangen- Nürnberg

Research Article

Keywords: Parkinson’s disease, alpha-synuclein, aggregation, oxidative stress, ROS, iPSC, dopaminergic neurons, mitochondria, NPT100-18A

Posted Date: May 30th, 2024

DOI: https://doi.org/10.21203/rs.3.rs-4400225/v1

Additional Declarations: Competing interest reported. WW is a cofounder of Neuropore Therapies, Inc. (San Diego, CA, USA). The other authors declare to have no conflict of interest.

Abstract

Background Parkinson's disease (PD) is a neurodegenerative disorder characterized by protein aggregates mostly consisting of misfolded alpha-synuclein (αSyn). Progressive degeneration of midbrain dopaminergic neurons (mDANs) and nigrostriatal projections result in severe motor symptoms. While the preferential loss of mDANs has not been fully understood yet, the cell type-specific vulnerability has been linked to a unique intracellular milieu, influenced by dopamine metabolism, high demand for mitochondrial activity, and increased level of oxidative stress (OS). These factors have been shown to adversely impact αSyn aggregation. Reciprocally, αSyn aggregates, in particular oligomers, can impair mitochondrial functions and exacerbate OS. Recent drug-discovery studies have identified a series of small molecules including NPT100-18A, which reduce αSyn oligomerization by preventing misfolding and dimerization. NPT100-18A and structurally similar compounds (such as NPT200-11/UCB0599, currently being assessed in clinical studies) point towards a promising new approach for disease-modification.

Methods Induced pluripotent stem cell (iPSC)-derived mDANs from PD patients with a monoallelic *SNCA* locus duplication and unaffected controls were treated with NPT100-18A. αSyn aggregation was evaluated biochemically and reactive oxygen species (ROS) levels were assessed in living mDANs using fluorescent dyes. Adenosine triphosphate (ATP) concentrations were measured using a luminescence-based assay and neuronal cell death was evaluated by immunocytochemistry.

Results Compared to controls, patient-derived mDANs exhibited increased αSyn aggregation, higher overall ROS levels, reduced ATP concentrations, and increased neuronal cell death. NPT100-18A-treatment rescued neuronal cell death to control levels and importantly attenuated mitochondrial oxidative stress in a compartment-specific manner.

Conclusions Our findings demonstrate that NPT100-18A limits αSyn aggregation and associated neurodegeneration in a human *in vitro* model of PD. In addition, we provide a first mechanistic insight into how a compartment-specific antioxidant effect in mitochondria might contribute to the neuroprotective effects of NPT100-18A.

Background

Parkinson's disease (PD) is a complex and progressive neurodegenerative disease with a markedly increasing incidence and global disease burden [1, 2]. PD is characterized by early and prominent loss of midbrain dopaminergic neurons (mDANs), resulting in disruption of nigrostriatal circuits. This results in motor symptoms encompassing hypo- and bradykinesia, muscular rigidity, and resting tremor [3]. Degeneration of mDANs is tightly connected to the intracellular accumulation of alpha-synuclein (αSyn)-containing protein aggregates, which reflect a neuropathological hallmark of PD [4].

Under physiological conditions, αSyn, encoded by *SNCA*, acts as a regulator of synaptic vesicle release and is enriched in presynaptic terminals. Within this compartment, αSyn cycles between a monomeric, highly soluble, and a membrane-bound multimeric state [5–9]. Increased expression of wild-type (WT) αSyn caused by copy number multiplications of the *SNCA* locus and single-nucleotide polymorphisms in non-coding enhancers of *SNCA*, have been linked to familial and idiopathic forms of PD [10–12]. Under these conditions, αSyn is prone to aggregate via oligomeric intermediate states towards large fibrillar aggregates, which solidify as Lewy bodies and Lewy neurites [13–16].

αSyn oligomers, a form of particularly toxic aggregates, are capable of impairing a multitude of cellular pathways including autophagy, proteasomal clearance, vesicle transport, as well as the endoplasmic reticulum (ER) and mitochondria [9, 9, 17–23]. In particular, the latter appear to be a preferential target of αSyn-mediated toxic effects [20, 24–27]. Dysfunctional mitochondria in turn act as catalysts for αSyn aggregation and neuronal cell death through reduced ATP regeneration, release of calcium, and excessive generation of reactive oxygen species (ROS) [20, 28]. This crucial link

between αSyn aggregation and mitochondrial dysfunction is further reflected by familial forms of PD, caused by pathologic variants in genes (e.g. DJ-1, PINK1 and PRKN) that regulate the mitochondrial oxidative stress (OS) response [29, 30]. In addition, we have previously shown that increased αSyn aggregation and ROS levels determine the cell type-specific vulnerability of mDANs in PD [31].

At present, no disease-modifying therapy for PD is available. However, important preclinical progress in targeting disease-relevant pathways has been made in recent years. Among the most promising approaches is NPT100-18A, a *de novo* compound identified in a structure-based drug-discovery [32]. The peptidomimetic small molecule inhibits protein-protein interaction between αSyn residues 96-102 and residues 80-90 of a complementary αSyn monomer. This prevents dimerization and propagation to toxic oligomers [32]. NPT100-18A and structurally similar compounds such as NPT200-11/UCB0599 (currently assessed in a clinical trial, NCT04658186) have been previously shown to reduce αSyn pathology, astrogliosis, and improve behavioral deficits in rodent *in vivo* models of PD. Furthermore, NPT100-18A treatment restored intact neurite morphology and mitochondrial axonal transport in human stem cell-based *in vitro* neuronal models expressing mutants of αSyn [23, 32–34]. However, to date, the molecular actions of NPT100-18A in human, WT αSyn-expressing dopaminergic neurons remain unclear.

This study investigates the effects of NPT100-18A in a human *in vitro* model of PD using induced pluripotent stem cell (iPSC)-derived neurons from patients with a monoallelic *SNCA* locus duplication. To study the effects of the compound on the aforementioned molecular drivers of PD neuropathology, αSyn, and mitochondrial dysfunction, as well as overall neuronal survival, we evaluated αSyn aggregation, ATP concentration, oxidative stress, and neuronal viability in mDANs differentiated from PD patient- and control-derived iPSCs.

Methods

Cells and cell culture

A total of five human iPSC lines were used. Two iPSC lines from PD patients bearing heterozygous *SNCA* locus duplication were kindly provided by Professor Galasko (line SDi1-R-C: clones SDi1-R-C3 and SDi1-R-C11 [23, 31]) and Dr. Roybon (line CSC-1: clones CSC-1A and CSC-1D [31, 35]). IPSCs from three age-matched healthy Caucasian individuals with no history of neurologic disease served as controls (cell lines UKERi82A-S1_017, UKERi33Q-R1-06, and UKERiO3H-R1, clones UKERiO3H-R1-001 and UKERiO3H-R1-005) and have been previously characterized [23, 31, 36]. IPSCs were differentiated through neural precursor cells (NPCs) into mDANs using a fibroblast growth factor 8 (FGF8)- and small molecule-based midbrain protocol previously described [31, 37]. NPCs were seeded onto Geltrex-coated 12-well plates and differentiated into mDANs using differentiation medium (50% DMEM/F12, 50% Neurobasal Medium, N2 [0.5x], B27 [0.5x]), supplemented with FGF-8b (100 ng/ml), purmorphamine (PMA, 1.2 µM) and ascorbic acid (200 nM). For maturation, cells were dissociated using accutase, seeded onto polyornithine/laminin-coated plates at $75x10^3/cm^2$ cell density and cultured for 14 days in differentiation medium supplemented with transforming growth factor beta-3 (TGF-β3, 1 ng/ml), glial cell-line derived neurotrophic factor (GDNF, 10 ng/ml), brain-derived neurotrophic factor (BDNF, 10 ng/ml), ascorbic acid (200 nM), and dibutyryl-cAMP (500 µM). During the first two days of maturation, 0.6 µM PMA was added to the medium. Contamination of the cell lines with mycoplasma was excluded routinely, using a PCR-based mycoplasma test. Reagents used are listed in Table S1.

NPT100-18A compound and treatment regimen

NPT100-18A is a *de novo* peptidomimetic compound with a cyclic pirimido-pyrazine scaffold developed and previously described by Wrasidlo et al. [32]. NPT100-18A was kindly provided by W. Wrasidlo and chemical purity was verified via LC-

MS. The compound was dissolved in DMSO at the concentration of 20 µM. NPT100-18A was added to the medium at a final concentration of 10 nM (or 100 nM for ATP quantification) starting from the first day of differentiation until the end of the maturation period. In parallel, mDANs were cultured under vehicle condition: differentiation/maturation medium with DMSO.

αSyn solubility assay and immunoblotting

Cells were manually homogenized in 1% Triton-X100-containing buffer (50 mM Tris-HCl pH 8.0, 150 mM NaCl, 1 mM EDTA, 1.5 mM MgCl2 with protease and phosphatase inhibitors). The lysate was separated into soluble and insoluble fractions by 20 minutes (min) centrifugation (18000xg, 4°C) and the insoluble pellet was resuspended in 0.5 M urea/5% SDS. For the soluble fraction, 10 µg of total protein in a total volume of 5 µl was spotted onto 0.2 µm nitrocellulose membrane, while for the insoluble fraction, 5 µl of the lysate was spotted. Membranes were air-dried for 2 hours (h) and subsequently fixed with 4% paraformaldehyde (PFA) for 20 min at room temperature (RT) to improve detection [38]. Membranes were blocked in 5% non-fat dry milk in Tris-buffered saline (TBS) containing 0.1% Tween 20 (TBST) for 1 h at RT and incubated with primary antibodies against aggregated and total αSyn (Table S1) diluted in 3% bovine serum albumin in TBST, followed by the appropriate horseradish peroxidase (HRP)-conjugated secondary antibodies. Chemiluminescent signal was detected with ECL Select on the Gel Doc XR system. Total protein loading was controlled by staining the membranes using 0.008% Direct Blue 71, 40% ethanol and 10% acetic acid for 5 min at RT, followed by de-staining with 150 mM sodium bicarbonate in 47.5% ethanol. Images were quantified using the FIJI software. The aggregated and total αSyn signals were normalized to total protein and the aggregated αSyn signal was subsequently normalized to total αSyn, followed by calculating the fraction of aggregated αSyn in soluble and insoluble fractions. Antibodies and reagents are listed in Table S1.

Immunocytochemistry and image acquisition

Immunocytochemistry and image acquisition were done as previously described [31, 36]. Briefly, cells were fixed using 4% PFA for 30 min at 37°C, permeabilized with ice-cold ethanol and acetic acid (2:1), washed three times with Dulbecco's phosphate-buffered saline (DPBS), and subsequently permeabilized and blocked using blocking solution (0.3% Triton-X100, 5% donkey serum in DPBS). Primary antibodies (diluted in blocking solution) were added overnight at 4°C. Fluorochrome-conjugated secondary antibodies were added for 1 h at RT. Cell nuclei were stained with 1 µg/ml 4',6-diamidino-2-phenylindole (DAPI). Coverslips with stained cells were mounted on glass microscope slides using Aqua Polymount. Images were acquired using an Axio Observer Z1 inverted fluorescence microscope and Zen Black Software. Images were evaluated blinded with regard to genotype and treatment of the cell line using the cell counter and blind analysis tool plugin for FIJI software [39]. Three independent differentiation rounds were done for each NPC line and at least three images were evaluated for each differentiation to assess neuronal cell death. Antibodies and reagents are listed in Table S1.

ROS measurements

Cytosolic and mitochondrial ROS levels were quantified in living mDANs as previously described [31]. Briefly, NPCs were seeded at a density of 50×10^3 cells per well in black 96-well plates with transparent flat bottom coated with polyornithine/laminin. On the final maturation day, mDANs were stained with CellROX Green or MitoSOX Red fluorescent dyes for detection of total intracellular ROS or mitochondrial superoxide, respectively. CellROX was added directly to the culture media at a concentration of 5 µM for 30 min at 37°C. Prior to incubation with MitoSOX neurons were washed once with warm DPBS (with Ca^{2+}/Mg^{2+}). MitoSOX (diluted in DPBS with Ca^{2+}/Mg^{2+}) was then added to the cells to a final concentration of 5 µM for 10 min at 37°C. After staining with CellRox or MitoSOX, DAPI (10 µg/ml, diluted in DPBS) was added for 5 min at 37°C and then cells were washed twice with warm DPBS. CellROX, MitoSOX, and DAPI fluorescence intensities were measured on a CLARIOstar Plus microplate reader (BMG Labtech) using the following

excitation/emission wavelengths: CellROX – 480-20/530-25 nm; MitoSOX – 510-15/580-20 nm; DAPI – 360-20/460-30 nm. A matrix scan protocol was used, measuring fluorescence intensities at 80 sites per well. CellROX and MitoSOX fluorescence intensities were normalized to DAPI for each site followed by normalization to the mean values of vehicle-treated control line C1. NPC lines were differentiated in four independent experiments. For each differentiation, neurons were cultured in quadruplicates at least. Reagents used are listed in Table S1.

ATP measurements

ATP levels in living mDANs were quantified as previously described [23]. NPCs were seeded at a density of 50×10^3 cells per well in white opaque 96-well plates coated with polyornithine/laminin. ATP measurements were performed using the luminescence-based CellTiter-Glo 2.0 Cell Viability Assay kit according to the manufacturer's instructions. Luminescence was measured using a LUMIstar Omega microplate reader. In parallel, neurons were differentiated under the same conditions in black 96-well plates with transparent flat bottom for viability testing using Image IT DEAD Green Viability Stain. Neurons were incubated with 100 nM IT DEAD Green reagent for 30 min at 37°C, fixed using 4% PFA and stained with DAPI (10 µg/ml diluted in DPBS). NPC lines were differentiated in three independent rounds. For each differentiation round, cells were cultured in duplicates at least. Three images were acquired for each well using an Axio Observer Z1 inverted fluorescence microscope. Relative ATP amount per cell was estimated by normalization of ATP signal to the frequency of viable cells. Mean ATP amounts in each well were normalized to the respective values of the vehicle-treated control line C1. Reagents used are listed in Table S1.

Statistics

Normality of distributions was assessed using D'Agostino-Pearson test and graphical methods and correspondingly, means and standard deviations are reported for continuous variables. Differences across groups were evaluated using two-way ANOVA followed by Tukey's post-hoc test for multiple comparisons, while differences between two groups were calculated using Student's t-test test or nested Student's t-test. Total intracellular ROS levels in DMSO/NPT-treated mDANs (Fig. 2A) and the percentage of DMSO/NPT-treated cCasp3/TH double positive neurons (Fig. 4B) were log-transformed to meet model assumptions. Statistical analyses were performed using Prism version 10.1.0 (GraphPad Prism). All statistical tests were two-sided and $P<0.05$ was considered significant. P values are denoted as follows: $P<0.05$ (∗), $P<0.01$ (∗∗), $P<0.001$ (∗∗∗) and $P<0.0001$ (∗∗∗∗).

Results

Increased αSyn aggregation coincides with increased ROS levels and mitochondrial dysfunction in PD patient-derived mDANs

We have previously reported the correlation of increased αSyn aggregation and oligomer levels and increased OS in mDANs from a PD patient (P2) [23, 31]. Before testing the effects of NPT100-18A (Fig. 1A), we first investigated the vulnerability of mDANs in additional PD patient- and control-derived mDAN lines (P1 and C1) and further characterized their mitochondrial phenotype. Detailed analyses of αSyn aggregation in these patient-derived lines have been reported in our previous work [31]. In the present study, we confirmed increased αSyn aggregation through immunoblotting for total and high-molecular weight αSyn aggregates in Triton X-100-soluble and -insoluble fractions of mDAN lysates (Fig. S1A). Next, we measured ROS levels in patient- and control-derived mDANs using CellRox and MitoSOX fluorescent probes to assess overall intracellular ROS and mitochondrial superoxide, respectively. As previously reported, fluorescent intensities were measured using a multi-mode microplate reader to ensure fast and simultaneous detection across multiple neuronal lines and conditions [31]. Overall intracellular ROS levels were 33.7% higher in patient- compared to control-derived mDANs ($P<0.0001$; Fig. 1B) with a concomitant increase of 17.2% in mitochondrial superoxide levels in

PD patient-derived mDANs (*P*<0.0001; Fig. 1D). After determining pronounced mitochondrial OS in patient-derived mDANs with increased WT αSyn expression, we next asked whether this might have an impact on mitochondrial function. Oxidative phosphorylation (OXPHOS) is a very well-characterized core mitochondrial function, known to be prone to changes of the intra-mitochondrial milieu and interference by αSyn oligomers [20, 25]. Consequently, we measured ATP concentrations as a proxy for OXPHOS using a luciferase-based assay. Relative ATP concentrations were significantly lower in patient- compared to control-derived mDANs (79.3% of control, *P*<0.0001; Fig. 1C).

Taken together, these results demonstrate a concomitant increase ofαSyn aggregation and oxidative stress burden in PD patient-derived mDANs and establish mitochondrial dysfunction as an additional contributor to neuropathology in this human *in vitro* PD model.

NPT100-18A reduces mitochondrial ROS levels in patient-derived mDANs

After demonstration of increased αSyn aggregation, oxidative stress, and mitochondrial dysfunction in the PD patient-derived mDAN line and, thus, characterizing a phenotype potentially amenable to treatment with NPT100-18A, we set out to investigate the effects of the novel small molecule on human iPSC-derived mDANs. Our treatment paradigm consisted of treatment with either 10 nM NPT100-18A or DMSO as a vehicle control during the whole differentiation and maturation period. Evaluation of αSyn aggregation revealed a trend towards reduced levels of Triton X-100-insoluble high-molecular weight αSyn species upon treatment with NPT100-18A, in both patient- and control-derived mDANs (Fig. S1B). Measuring total intracellular ROS levels using CellRox fluorescent probe in living neurons, we did not find a significant effect of NPT100-18A- compared to DMSO-treatment, in either patient- or control-derived mDANs with overall higher ROS levels in patient-derived mDANs compared to controls (Fig. 2A). Mitochondria are considered a major source of ROS production in neural cells and toxic oligomers of A53T mutant and WT αSyn have been shown to specifically increase mitochondrial oxidative damage [20, 40]. Therefore, we asked whether NPT100-18A-mediated reduction of αSyn aggregation, while not impacting overall intracellular OS level, may have a mitochondria-specific effect on ROS generation. To address this question, we measured mitochondrial superoxide in living mDANs as described above using a MitoSOX fluorescent probe. Treatment with 10 nM NPT100-18A indeed significantly reduced mitochondrial ROS levels compared to vehicle control (88.4% of control, *P*=0.0071, two-way ANOVA; Fig. 2B). Importantly, mitochondrial ROS levels of control-derived mDANs were not significantly affected by the NPT100-18A treatment. Next, we measured ATP concentrations, to test whether NPT100-18A might also alleviate mitochondrial dysfunction. While treatment with 10 nM NPT100-18A did not influence ATP concentrations (data not shown), we observed a numerical trend towards increased relative ATP concentrations upon treatment with 100 nM NPT100-18A (*P*=0.10, two-way ANOVA; Fig. 2C).

NPT100-18A rescues increased rates of neuronal cell death in patient-derived mDANs

After determining the protective effects of NPT100-18A on intramitochondrial ROS, we next aimed to assess the compound's capacity to protect patient-derived mDANs from αSyn-mediated neurodegeneration. To evaluate the efficacy of NPT100-18A treatment on preventing loss of mDANs, we first established a baseline for neuronal cell death in untreated patient- and control-derived neurons. For this, basal neuronal death rate was quantified through immunocytochemistry, staining for cleaved Caspase-3 (cCasp3), an established marker of neuronal cell death [41], in neurons double-positive for β3-tubulin (TUBB3) and tyrosine hydroxylase (TH; Fig. 3A-B and Fig. S2A). IPSC-derived mDANs from two PD patients with *SNCA* locus duplication (two iPSC-clones per patient; Tab. 1) and three control individuals (one iPSC-clone for C1 and C2, and two iPSC-clones for C3; Tab. 1) were examined. The pooled mean percentage of apoptotic mDANs was significantly higher in patient- compared to control-derived mDANs (11.9% vs. 3.2%, respectively, nested t-test, *P*=0.0003) with no significant differences across either patient or control neuronal lines

(χ^2=0.77, *P*=0.38; Fig. 3C). Next, we evaluated the effects of NPT100-18A-treatment on neuronal cell death. MDANs were treated with either 10 nM NPT100-18A or DMSO starting on the first day of differentiation and the rate of neuronal death was assessed after 21 days of treatment. Treatment with the NPT100-18A compound significantly reduced the rates of dying neurons compared to DMSO-treatment in mDANs from both patients (pooled rates: 4.2% vs. 14.4%, nested t-test, *P*=0.0041; P1.1: 3.4% vs. 12.8%, *P*<0.0001, P1.2: 4.9% vs 17.1%, *P*<0.0033, P2.1: 4.9% vs 15.3%, *P*=0.0002, P2.2: 4.6% vs. 15.1%, *P*=0.0008; two-way ANOVA; Fig. 4A-B and Fig. S2B). NPT100-18A-treatment of patient-derived mDANs reduced neuronal cell death to the level of DMSO-treated control-derived mDANs (pooled mean mDAN death rate 4.1% vs. 3.7%, respectively, nested t-test, *P*=0.57). No significant effect of NPT100-18A-treatment on neuronal cell death was observed in control-derived mDANs (Fig. 4B).

Altogether, these results reveal increased levels of neuronal cell death in PD patient-derived mDANs and demonstrate that NPT100-18A limits neuronal cell death caused by increased αSyn aggregation, essentially reducing the frequencies of dying mDANs to those of untreated control neurons (Fig. 5).

Discussion

The peptidomimetic small molecule NPT100-18A and its derivatives pose a promising, new and causal therapeutic approach for PD. By inhibiting protein-protein interaction between the C-termini of αSyn monomers, the compound prevents the formation of toxic αSyn oligomers [32]. In this study, we set out to examine the effects of NPT100-18A on human iPSC-derived mDANs. Establishing increased αSyn aggregation, increased ROS levels, mitochondrial dysfunction, and increased neuronal cell death, we recapitulate neuropathological hallmarks of PD in human iPSC-derived mDANs from patients with a monoallelic *SNCA* locus duplication and characterize a phenotype potentially amenable to treatment with the αSyn misfolding inhibitor. We subsequently demonstrate that reduction of αSyn aggregation through treatment with NPT100-18A specifically reduces mitochondrial ROS levels and rescues neuronal cell death in patient-derived neurons. We thereby show the efficacy of the misfolding inhibitor in limiting loss of mDANs, for the first time in a human iPSC-derived model of PD and provide a first mechanistic insight into how a mitochondria-specific antioxidant effect might elicit its neuroprotective effects.

Recent studies have revealed a causal link between neurotoxic αSyn oligomers, disruption of normal mitochondrial function and oxidative stress at several levels. αSyn oligomers have been shown to interfere with complex I of the electron transport chain (ETC) and ATP synthase and thereby directly induce mitochondrial bioenergetic defects [20, 25]. In line with this, in the present study, we found significantly reduced ATP concentrations in patient-derived mDANs with monoallelic *SNCA* locus duplication and increased αSyn aggregation. While mitochondrial dysfunction and reduced ATP regeneration pose a significant challenge to all neuronal subpopulations, mDANs seem to be particularly vulnerable due to the intertwining of monoamine oxidase (MAO)-dependent dopamine (DA) metabolism and ETC activity. Electrons released during degradation of DA, which under physiological conditions are shuttled into the mitochondrial intermembrane space and contribute to ATP regeneration, become available to form intramitochondrial and cytoplasmic ROS upon uncoupling of MAO and the ETC [42]. We previously reported increased ROS levels to be an important determinant of the cell type-specific vulnerability of mDANs in PD, differentiating them from other non-dopaminergic neuronal subpopulations, such as cortical projection neurons [31]. Here, we found both overall intracellular and mitochondrial ROS levels to be significantly increased in patient-derived compared to control mDANs. Furthermore, αSyn oligomer-induced exacerbation of intramitochondrial ROS burden can result in opening of permeability transition pore (PTP) [20]. Opening of PTP triggers changes in mitochondrial membrane potential, calcium homeostasis, and release of cytochrome C, eventually leading to activation of executioner caspases and neuronal cell death [20, 43]. In accordance with this, in patient-derived mDANs, we observed significantly increased rates of neurons positive for cCaspase 3, an

important executioner caspase and well-established marker of neuronal cell death. In summary, we demonstrate that this model recapitulates pathological features deemed pivotal in the mDAN-specific neurodegenerative cascade in PD.

Considering that aSyn aggregation has been recognized as a key driver of neuropathology in PD and its intertwining with DA metabolism and mitochondrial dysfunction, we hypothesized that interference with αSyn aggregation might ameliorate the cellular phenotype characterized above and thereby prevent loss of patient-derived mDANs.

Among the most promising inhibitors of αSyn aggregation is NPT100-18A, a small molecule which prevents αSyn oligomerization by blocking protein-protein interaction of αSyn monomers. NPT100-18A has been previously tested in αSyn transgenic rodent models of PD (primary cortical neurons with lentiviral αSyn overexpression and mThy1-WT-αSyn transgenic mice) and an A53T-mutant αSyn-expressing iPSC-derived model of PD [32, 34]. In these models, treatment with the misfolding inhibitor reduced αSyn aggregation and ameliorated morphological defects of neurites *in vitro* as well as behavioral deficits *in vivo* [32, 34]. In addition, we previously demonstrated reduced αSyn oligomerization and rescue of axonal transport defects upon treatment in iPSC-derived mDANs transduced with mutant or WT αSyn [23]. However, to date, no comprehensive characterization of the effects of NPT100-18A in a human model with physiologically increased WT αSyn expression has been reported.

To fill the gap in knowledge of NPT100-18A effects in human dopaminergic neurons, we chose iPSC-derived mDANs from patients with monoallelic *SNCA* locus duplication as a WT αSyn overexpressing model of PD. As the impact of NPT100-18A on WT αSyn aggregation has been previously characterized in detail [23, 32], we focused on potential downstream effects of the small molecule-mediated reduction of αSyn oligomers. Using fluorescent probes in living mDAN cultures, revealed a robust and statistically significant reduction of mitochondrial ROS levels in treated, patient-derived neurons, while no effect on overall intracellular ROS levels was noticeable. Although the observed trend towards increased of ATP concentrations did not reach statistical significance, factoring in the volatility of singular measurements of ATP and the presumed downstream effect on ROS levels evident in mitochondria, we considered this to generally be in line with our hypothesis. However, further studies will be needed to comprehensively characterize the effects of NPT100-18A-treatment on a wider array of parameters defining mitochondrial integrity. To further test whether the observed reduction in αSyn aggregation could prevent loss of human dopaminergic neurons *in vitro*, we performed immunocytochemical staining, which revealed a significantly reduced rate of neuronal cell death in NPT100-18A-treated mDANs. Notably, treated patient-derived mDANs showed rates of cCasp3-positive neurons comparable to those of control-derived mDANs. Degeneration of mDANs and subsequent disruption of nigrostriatal circuits is considered one of the most important pathological hallmarks of PD and causative for the development of disabling motor symptoms [44–46]. Here, we demonstrate that NPT100-18A treatment can limit the loss of dopaminergic neurons in a human *in vitro* model of PD.

Conclusion

In conclusion, we demonstrate that administration of αSyn misfolding inhibitor NPT100-18A reduces loss of mDANs in a human *in vitro* model of PD. In addition, we provide a first mechanistic insight into how a compartment-specific antioxidant effect in mitochondria might mediate the neuroprotective effects of NPT100-18A in human dopaminergic neurons.

Abbreviations

ATP - adenosine triphosphate

BDNF - brain-derived neurotrophic factor

C - control

cCasp3 - cleaved Caspase-3

DA - dopamine

DAPI - 4',6-diamidino-2-phenylindole

DPBS - Dulbecco’s phosphate-buffered saline

ER - endoplasmic reticulum

ETC - electron transport chain

FGF8 - fibroblast growth factor 8

GDNF - glial cell-line derived neurotrophic factor

h - hours

HRP - horseradish peroxidase

iPSC - induced pluripotent stem cell

MAO - monoamine oxidase

mDANs - midbrain dopaminergic neurons

min - minutes

NPCs - neural precursor cells

OS - oxidative stress

P - patient

PD - Parkinson’s disease

PFA - paraformaldehyde

PMA - purmorphamine

PTP - permeability transition pore

ROS - reactive oxygen species

RT - room temperature

SNCA - αSyn gene

TBS - Tris-buffered saline

TBST - TBS containing 0.1% Tween 20

TGF-β3 - transforming growth factor beta-3

TH - tyrosine hydroxylase

TUBB3 - β3-tubulin

WT - wild-type

αSyn - alpha-synuclein

Declarations

Ethics approval and consent to participate

The study was performed in accordance with the Declaration of Helsinki. Human iPSCs derived from human dermal fibroblasts were obtained from the stem cell unit of the Friedrich-Alexander University Erlangen-Nürnberg. Written informed consent was received from voluntary donors of skin biopsies prior to inclusion in the study at the Movement Disorder Clinic at the Department of Molecular Neurology, University Hospital Erlangen. All experiments using human iPSC-derived cells were conducted in accordance with the Institutional Review Board approval (Nr. 259_17B), as well as national and European Union directives. The iPSC line CSC-1 was generated from fibroblasts obtained with informed consent and after ethical committee approval at the Parkinson Institute in Milan. The permit for reprogramming of CSC-1 was delivered by the Swedish Work Environment Authority (Arbetsmiljöverket, reg.-no.: 20200-3211).

Consent to publish

Study participant names and other personally identifiable information were removed from all text/figures/tables/images. Written informed consent for publication was received from all donors prior inclusion into the study.

Availability of data and materials

Data are available from the corresponding authors upon reasonable request.

Competing interests

WW is a cofounder of Neuropore Therapies, Inc. (San Diego, CA, USA). The other authors declare to have no conflict of interest.

Funding

This work was supported by Deutsche Forschungsgemeinschaft (DFG, German Research Foundation) (270949263/GRK2162 to JEA, VS, RMB, MR, and BW; 505539112/KFO5024 to BW and IP; GRK2599 to IP; 535375124 to KMG); the Fritz Thyssen Foundation (10.19.2.024MN to IP), Johannes and Frieda Marohn Foundation (to IP) , and ELAN Fonds of the University Hospital of Erlangen (P117 to IP); Swedish research council and the Crafoord Foundation (to LR); German Academic Scholarship Foundation, the Max Weber-Program of the State of Bavaria and the German National Exchange Service (to JEA); Bavarian Ministry of Research and the Arts in the framework of the ForInter network.

Author contributions

JEA, VS, IP, KMG, LR, WW, and BW conceptualized and designed the experiments. JEA, VS, RMB, MB, IP, and SL performed the experiments and analyzed data. JEA, VS, and SL performed the statistical analysis. LR provided iPSC lines from P1, MR provided control fibroblast lines. WW provided NPT100-18A. JEA, BW and IP drafted the original

manuscript, with contributions from other authors. All authors critically revised the manuscript and approved the submitted version.

Authors' information

The present work was performed in fulfillment of the requirements for obtaining the degree ‘Dr. med.’ for Julian E. Alecu.

Acknowledgements

The authors thank the patients and their families who participated in this study. The authors would like to acknowledge Annika Sommer and Steven Havlicek for providing iPSC-derived NPCs and Douglas Galasko for providing iPSC lines from P2. The authors thank Daniela Graef and Holger Wend for excellent technical support. The present work was performed in fulfillment of the requirements for obtaining the degree ‘Dr. med.’ for Julian E. Alecu.

References

1. Ou Z, Pan J, Tang S, et al. Global Trends in the Incidence, Prevalence, and Years Lived With Disability of Parkinson's Disease in 204 Countries/Territories From 1990 to 2019. Frontiers in public health 2021;9:776847.
2. Dorsey ER, Elbaz A, Nichols E, et al. Global, regional, and national burden of Parkinson's disease, 1990–2016: a systematic analysis for the Global Burden of Disease Study 2016. The Lancet Neurology 2018;17:939–953.
3. Kalia LV, Lang AE. Parkinson's disease. Lancet (London, England) 2015;386:896–912.
4. Spillantini MG, Schmidt ML, Lee VM, et al. Alpha-synuclein in Lewy bodies. Nature 1997;388:839–840.
5. Burré J, Sharma M, Südhof TC. Cell Biology and Pathophysiology of α-Synuclein. Cold Spring Harbor perspectives in medicine 2018;8.
6. Burré J, Sharma M, Tsetsenis T, et al. Alpha-synuclein promotes SNARE-complex assembly in vivo and in vitro. Science (New York, N.Y.) 2010;329:1663–1667.
7. Bartels T, Choi JG, Selkoe DJ. α-Synuclein occurs physiologically as a helically folded tetramer that resists aggregation. Nature 2011;477:107–110.
8. Selkoe D, Dettmer U, Luth E, et al. Defining the native state of α-synuclein. Neuro-degenerative diseases 2014;13:114–117.
9. Du X-Y, Xie X-X, Liu R-T. The Role of α-Synuclein Oligomers in Parkinson's Disease. International journal of molecular sciences 2020;21.
10. Chartier-Harlin M-C, Kachergus J, Roumier C, et al. α-synuclein locus duplication as a cause of familial Parkinson's disease. The Lancet 2004;364:1167–1169.
11. Singleton AB, Farrer M, Johnson J, et al. alpha-Synuclein locus triplication causes Parkinson's disease. Science (New York, N.Y.) 2003;302:841.
12. Soldner F, Stelzer Y, Shivalila CS, et al. Parkinson-associated risk variant in distal enhancer of α-synuclein modulates target gene expression. Nature 2016;533:95–99.
13. Delenclos M, Burgess JD, Lamprokostopoulou A, et al. Cellular models of alpha-synuclein toxicity and aggregation. Journal of neurochemistry 2019; DOI:10.1111/jnc.14806.
14. Alam P, Bousset L, Melki R, et al. α-synuclein oligomers and fibrils: a spectrum of species, a spectrum of toxicities. Journal of neurochemistry 2019;150:522–534.
15. Rockenstein E, Nuber S, Overk CR, et al. Accumulation of oligomer-prone α-synuclein exacerbates synaptic and neuronal degeneration in vivo. Brain a journal of neurology 2014;137:1496–1513.

16. Cremades N, Chen SW, Dobson CM. Structural Characteristics of α-Synuclein Oligomers. International review of cell and molecular biology 2017;329:79–143.
17. Outeiro TF, Lindquist S. Yeast cells provide insight into alpha-synuclein biology and pathobiology. Science (New York, N.Y.) 2003;302:1772–1775.
18. Fusco G, Chen SW, Williamson PTF, et al. Structural basis of membrane disruption and cellular toxicity by α-synuclein oligomers. Science (New York, N.Y.) 2017;358:1440–1443.
19. Lindersson E, Beedholm R, Højrup P, et al. Proteasomal inhibition by alpha-synuclein filaments and oligomers. The Journal of biological chemistry 2004;279:12924–12934.
20. Ludtmann MHR, Angelova PR, Horrocks MH, et al. α-synuclein oligomers interact with ATP synthase and open the permeability transition pore in Parkinson's disease. Nature communications 2018;9:2293.
21. Chen L, Jin J, Davis J, et al. Oligomeric alpha-synuclein inhibits tubulin polymerization. Biochemical and biophysical research communications 2007;356:548–553.
22. Wong YC, Krainc D. α-synuclein toxicity in neurodegeneration: mechanism and therapeutic strategies. Nature medicine 2017;23:1–13.
23. Prots I, Grosch J, Brazdis R-M, et al. α-Synuclein oligomers induce early axonal dysfunction in human iPSC-based models of synucleinopathies. Proceedings of the National Academy of Sciences of the United States of America 2018;115:7813–7818.
24. Chinta SJ, Mallajosyula JK, Rane A, et al. Mitochondrial α-synuclein accumulation impairs complex I function in dopaminergic neurons and results in increased mitophagy in vivo. Neuroscience letters 2010;486:235–239.
25. Luth ES, Stavrovskaya IG, Bartels T, et al. Soluble, prefibrillar α-synuclein oligomers promote complex I-dependent, Ca2+-induced mitochondrial dysfunction. The Journal of biological chemistry 2014;289:21490–21507.
26. Wang X, Becker K, Levine N, et al. Pathogenic alpha-synuclein aggregates preferentially bind to mitochondria and affect cellular respiration. Acta neuropathologica communications 2019;7:41.
27. Di Maio R, Barrett PJ, Hoffman EK, et al. α-Synuclein binds to TOM20 and inhibits mitochondrial protein import in Parkinson's disease. Science translational medicine 2016;8:342ra78.
28. Cenini G, Lloret A, Cascella R. Oxidative Stress in Neurodegenerative Diseases: From a Mitochondrial Point of View. Oxidative medicine and cellular longevity 2019;2019:2105607.
29. Bonifati V, Rizzu P, van Baren MJ, et al. Mutations in the DJ-1 gene associated with autosomal recessive early-onset parkinsonism. Science (New York, N.Y.) 2003;299:256–259.
30. Trempe J-F, Fon EA. Structure and Function of Parkin, PINK1, and DJ-1, the Three Musketeers of Neuroprotection. Frontiers in neurology 2013;4:38.
31. Brazdis R-M, Alecu JE, Marsch D, et al. Demonstration of brain region-specific neuronal vulnerability in human iPSC-based model of familial Parkinson's disease. Human molecular genetics 2020;29:1180–1191.
32. Wrasidlo W, Tsigelny IF, Price DL, et al. A de novo compound targeting α-synuclein improves deficits in models of Parkinson's disease. Brain 2016;139:3217–3236.
33. Price DL, Koike MA, Khan A, et al. The small molecule alpha-synuclein misfolding inhibitor, NPT200-11, produces multiple benefits in an animal model of Parkinson's disease. Scientific Reports 2018;8:16165.
34. Kouroupi G, Taoufik E, Vlachos IS, et al. Defective synaptic connectivity and axonal neuropathology in a human iPSC-based model of familial Parkinson's disease. PNAS 2017;114:E3679-E3688.
35. Holmqvist S, Lehtonen Š, Chumarina M, et al. Creation of a library of induced pluripotent stem cells from Parkinsonian patients. NPJ Parkinson's disease 2016;2:16009.
36. Simmnacher K, Krach F, Schneider Y, et al. Unique signatures of stress-induced senescent human astrocytes. Experimental neurology 2020;334:113466.

37. Reinhardt P, Glatza M, Hemmer K, et al. Derivation and expansion using only small molecules of human neural progenitors for neurodegenerative disease modeling. PloS one 2013;8:e59252.
38. Sasaki A, Arawaka S, Sato H, et al. Sensitive western blotting for detection of endogenous Ser129-phosphorylated α-synuclein in intracellular and extracellular spaces. Scientific Reports 2015;5:14211.
39. Schindelin J, Arganda-Carreras I, Frise E, et al. Fiji: an open-source platform for biological-image analysis. Nature methods 2012;9:676–682.
40. Di Hu, Sun X, Liao X, et al. Alpha-synuclein suppresses mitochondrial protease ClpP to trigger mitochondrial oxidative damage and neurotoxicity. Acta neuropathologica 2019;137:939–960.
41. Yakovlev AG, Faden AI. Mechanisms of neural cell death: implications for development of neuroprotective treatment strategies. NeuroRx the journal of the American Society for Experimental NeuroTherapeutics 2004;1:5–16.
42. Graves SM, Xie Z, Stout KA, et al. Dopamine metabolism by a monoamine oxidase mitochondrial shuttle activates the electron transport chain. Nature neuroscience 2020;23:15–20.
43. Kinnally KW, Antonsson B. A tale of two mitochondrial channels, MAC and PTP, in apoptosis. Apoptosis an international journal on programmed cell death 2007;12:857–868.
44. Dickson DW, Braak H, Duda JE, et al. Neuropathological assessment of Parkinson's disease: refining the diagnostic criteria. The Lancet. Neurology 2009;8:1150–1157.
45. Kordower JH, Olanow CW, Dodiya HB, et al. Disease duration and the integrity of the nigrostriatal system in Parkinson's disease. Brain 2013;136:2419–2431.
46. Winter Y, Campenhausen S von, Arend M, et al. Health-related quality of life and its determinants in Parkinson's disease: results of an Italian cohort study. Parkinsonism & Related Disorders 2011;17:265–269.
47. Havlicek S, Kohl Z, Mishra HK, et al. Gene dosage-dependent rescue of HSP neurite defects in SPG4 patients' neurons. Hum Mol Genet 2014;23:2527–2541.
48. Sommer A, Marxreiter F, Krach F, et al. Th17 Lymphocytes Induce Neuronal Cell Death in a Human iPSC-Based Model of Parkinson's Disease. Cell stem cell 2018;23:123-131.e6.

Tables

Table 1 – Probands and iPSC lines

Proband	Abbreviation cell line	iPSC line name	Gender	Ethnicity	Age at biopsy (y)	Diagnosis	Genotype	Reference
P1	P1.1	CSC1-A	Female	Caucasian	53	Early-onset PD	Monoallelic *SNCA* locus duplication	31, 35, 36
	P1.2	CSC1-D						
P2	P2.1	SDi1-R-C3	Female	Caucasian	58	Early-onset PD	Monoallelic *SNCA* locus duplication	23, 35, 36, 47
	P2.2	SDi1-R-C11						
C1	C1	UKERi82A-S1_017	Female	Caucasian	66	Unaffected control	*SNCA* wildtype	36
C2	C2	UKERi33Q-R1-06	Female	Caucasian	45	Unaffected control	*SNCA* wildtype	23, 31, 36, 47
C3	C3.1	UKERiO3H-R1-001	Male	Caucasian	71	Unaffected control	*SNCA* wildtype	23, 31, 36, 47, 48
	C3.2	UKERiO3H-R1-005						

Figures

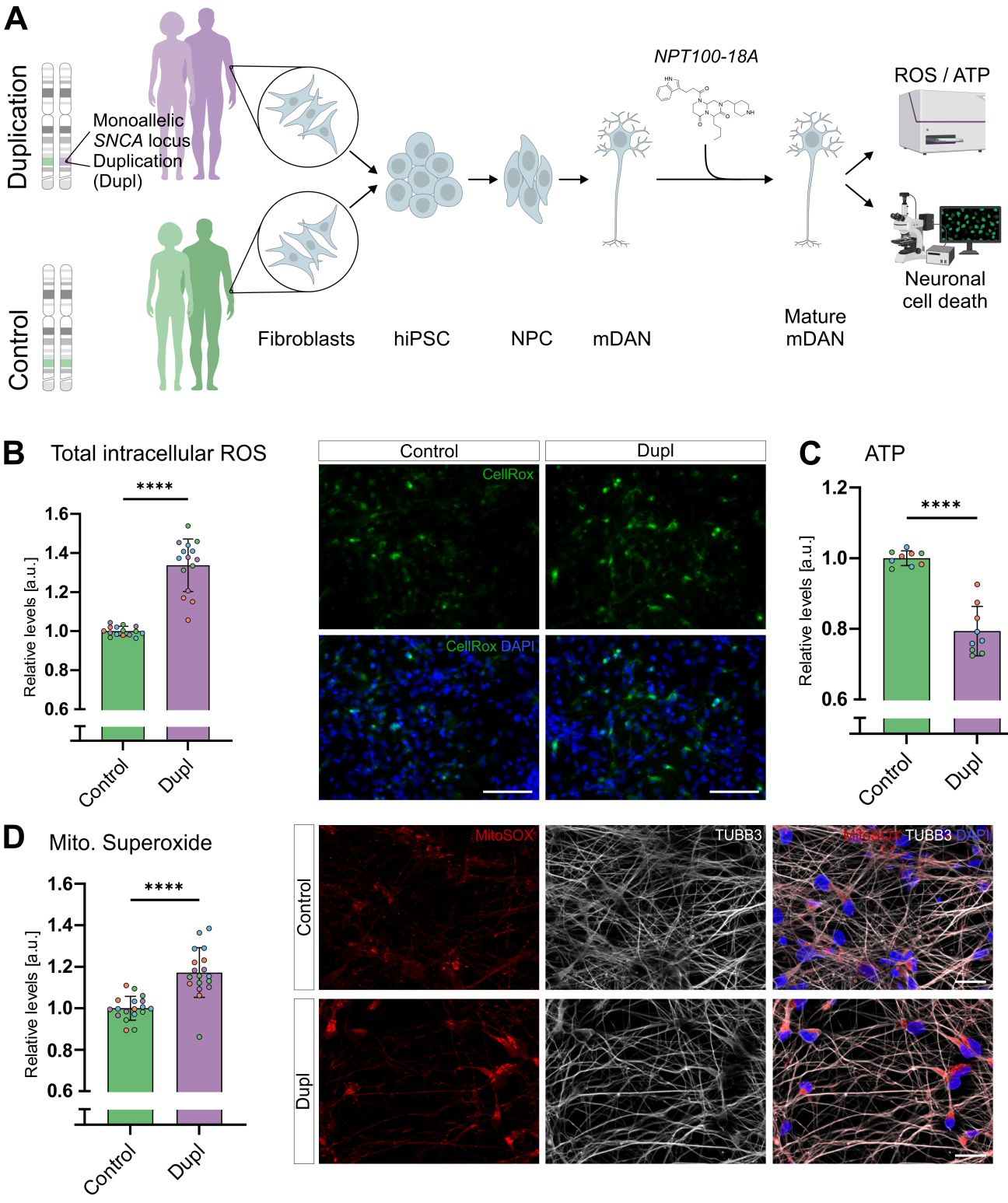

Figure 1

Increased oxidative stress and mitochondrial dysfunction in patient-derived mDANs. (**A**) Schematic of the experimental design. Fibroblasts from PD patients carrying a monoallelic *SNCA* locus duplication and unaffected control individuals were obtained through punch biopsy of the skin. Fibroblasts were reprogrammed into human iPSCs. Human iPSCs were first differentiated into NPCs through dual SMAD inhibition and activation of canonical Wnt signaling and then into mDANs using a FGF8b-based protocol. mDANs were treated with NPT100-18A during whole differentiation and maturation periods. (**B-D**) Relative levels depicted as fold change from the mean of control cell line C1 ± SD of n wells

from N independent differentiations. (**B**) Overall intracellular ROS levels were assessed using CellRox Green reagent in living mDANs. CellRox and DAPI fluorescence intensities (FIs) were measured at 80 sites per well in 96-well plates using a CLARIOstar plate reader. CellRox FIs were normalized to respective DAPI FIs. Dots representing single well means (n=15, N=4). Right panels show representative microscopy images of CellRox and DAPI fluorescence signals. (**C**) Significantly reduced ATP concentrations measured in patient-derived compared to control mDANs. Relative ATP concentrations were assessed in mDAN lysates using a luciferase-based assay and a LUMIstar Omega plate reader. Values for single wells were normalized to the frequency of viable neurons (determined with a viability staining in mDANs cultured in parallel under the same conditions). Dots representing single wells (n=9, N=3). (**D**) Mitochondrial superoxide was measured in living mDANs analogously to (B), using MitoSOX Red fluorescent mitochondrial superoxide indicator. Dots representing single well means (n=18, N=4). Right panels show representative microscopy images of MitoSOX and DAPI fluorescence signals; for better visualization of neurons, β3-tubulin (TUBB3) was additionally immunofluorescently labelled. (**B-D**) student's t-test, ****$P < 0.0001$. Scale bar 50 µm in (B) and 20 µm in (D).

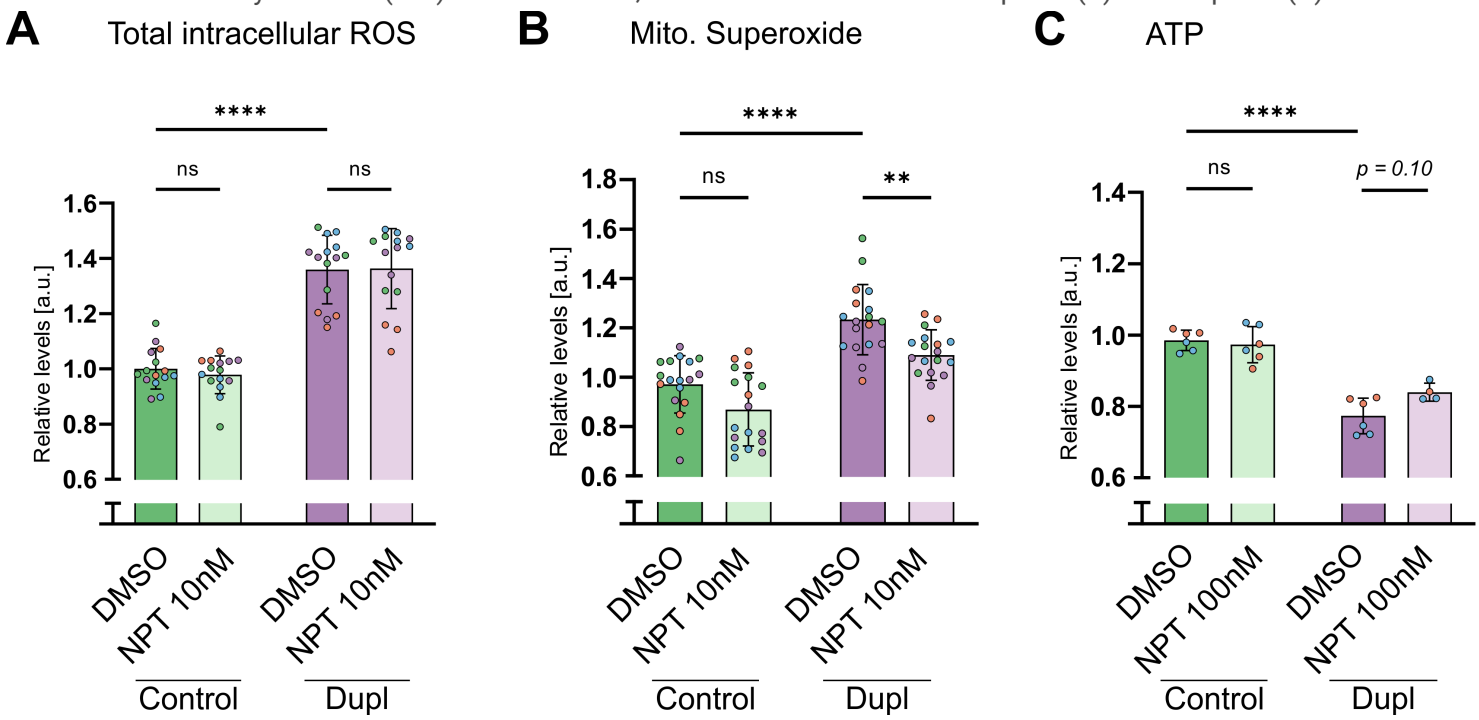

Figure 2

Treatment with NPT100-18A reduces mitochondrial ROS levels. (**A-C**) Relative levels depicted as fold change from the mean of untreated control cell line C1 ± SD of n wells from N independent differentiations. (**A**) Treatment with 10 nM NPT100-18A had no significant effect on total intracellular ROS levels in proband- and control-derived mDANs. Total intracellular ROS was quantified and depicted analogously to (Fig. 2A) with dots representing well means (n=15, N=4). (**B**) Treatment with 10 nM NPT100-18A significantly reduced mitochondrial superoxide in patient-derived but not in control mDANs (n=18, N=4). (**C**) Treatment with 100 nM NPT100-18A had no significant effect on ATP concentrations in proband- and control-derived mDANs (n=6, N=2); for the P1.1 with NPT100-18A-treatment condition two outliers showing excessively high ATP concentrations were excluded from further analysis (datapoints not shown). (A-C) two-way ANOVA with Tukey's post-hoc test for multiple comparisons, ns = not significant, **$P < 0.01$, ****$P < 0.0001$.

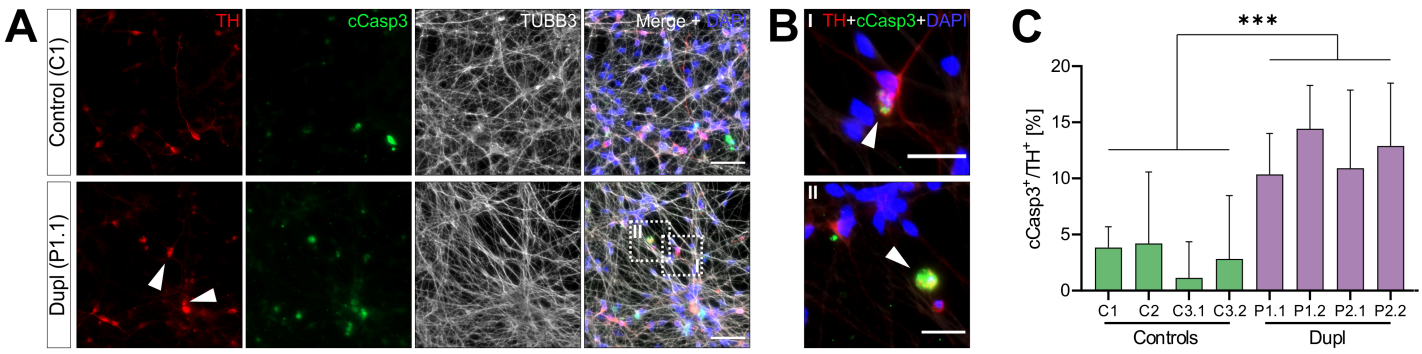

Figure 3

PD patient-derived mDANs show increased neuronal cell death. (**A**) Untreated iPSC-derived mDANs ($TUBB3^+/TH^+$) from patients and controls were stained for cleaved Caspase-3 (cCasp3) for evaluation of neuronal cell death. Representative images used for the quantification (C) are shown. Arrows indicate $TUBB3^+/TH^+/cCasp3^+$ neurons. (**B**) Enlarged views of selected cells marked by white frames in (A), showing a neuron considered as dying $TUBB3^+/TH^+/cCasp3^+$ (I) and a $cCasp3^+$ structure not considered a dying neuron (II). (**C**) Immunocytochemistry quantification. mDANs from two PD patients (with two different iPSC clones for each patient: P1.1, P1.2 and P2.1, P2.2) and three control individuals (with one iPSC clone for control 1 [C1] and 2 [C2] and two clones for control 3: C3.1 and C3.2). Patient-derived mDANs exhibit significantly higher neuronal cell death rates than controls. Two-tailed nested t-test ***P=0.0008; mean control = 3.68%, mean patient = 12.14%; no significant differences between subgroups, χ^2 P=0.56. Values are shown as mean ± SD of three independent differentiations. Scale bar 50 µm in (A) and 20 µm in (B).

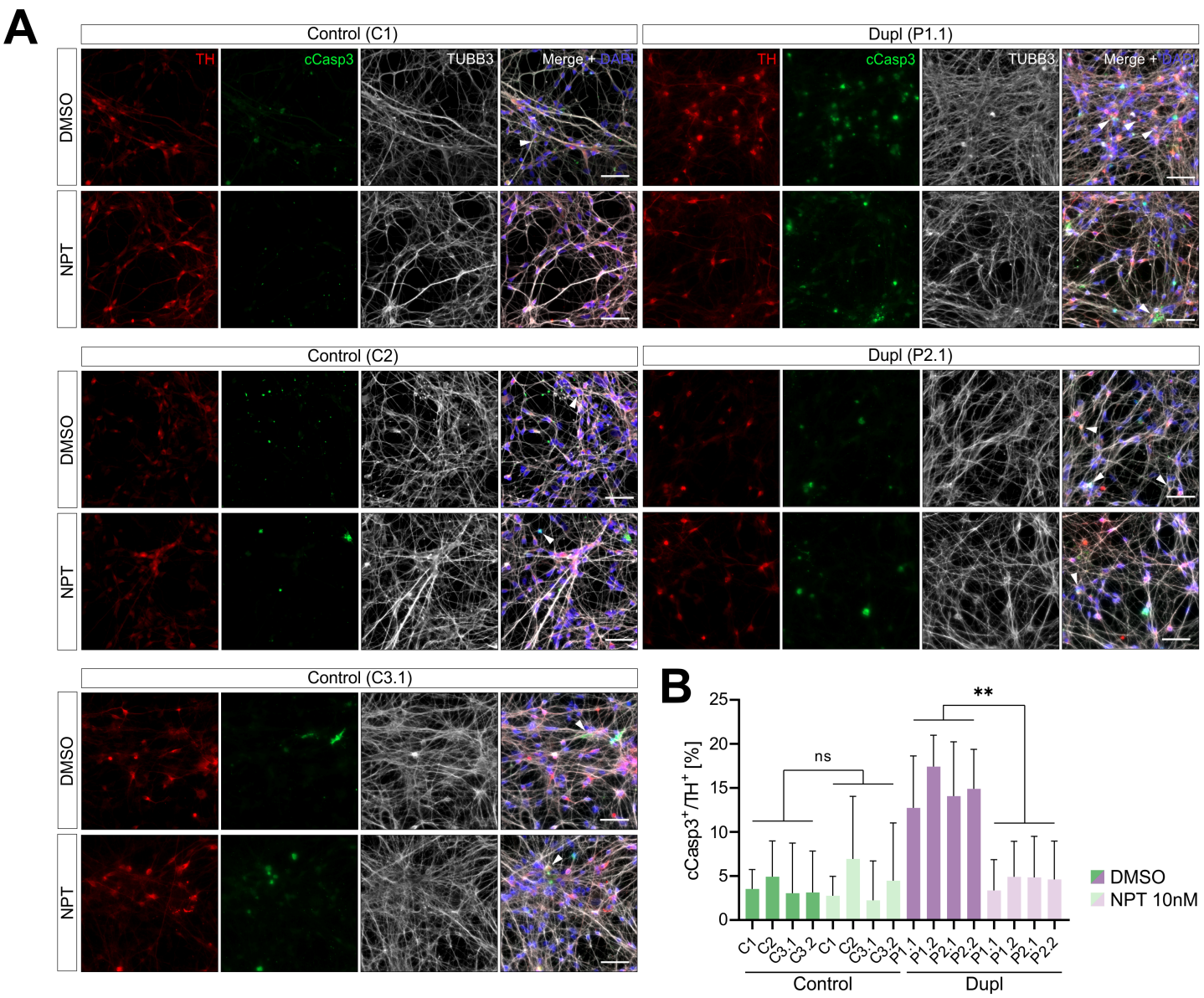

Figure 4

Increased neuronal cell death in PD patient-derived mDANs is reversed by treatment with NPT100-18A. (**A**) NPT100-18A- and DMSO-treated iPSC-derived mDANs ($TUBB3^+/TH^+$) from PD patients and controls were stained for cleaved Caspase-3 (cCasp3) to evaluate neuronal cell death rates. Representative images used for quantification (B) are shown. Scale bar 50µm. (**B**) Immunocytochemistry quantification. mDANs from two PD patients (P) (with two different iPSC-clones for each patient) and three control individuals (with one iPSC clone for control [C] 1 and 2 and two clones for C3). Treatment with 10 nM of NPT100-18A significantly reduced neuronal cell death rates compared to vehicle condition in all patient-derived but not in control mDAN lines. Two-way ANOVA with Tukey's post-hoc test for multiple comparisons; ns = not significant, ***P<0.001, ****P<0.0001. Values are shown as mean ± SD of three independent differentiations. Scale bar 50µm.

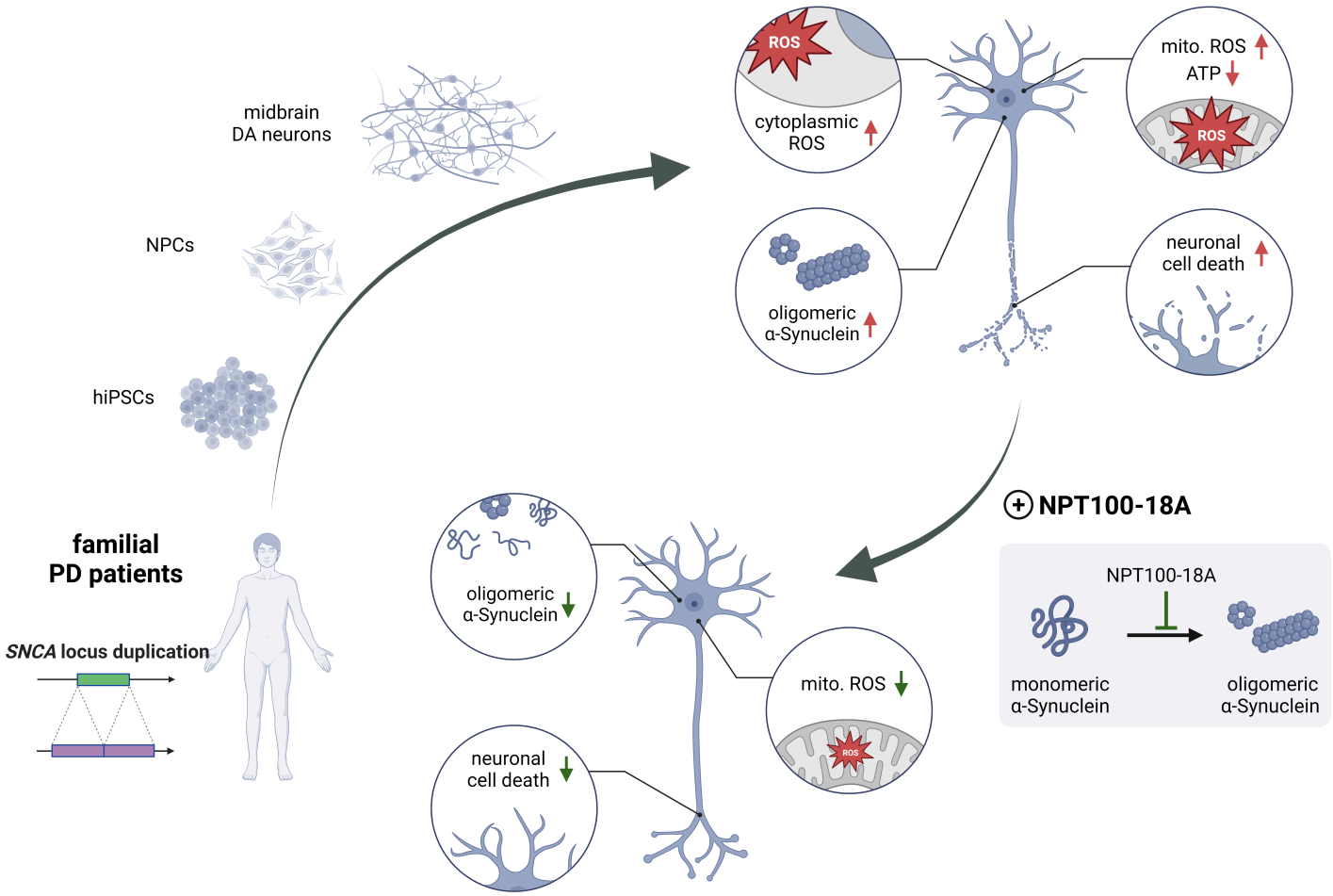

Figure 5

Graphical abstract of the study. Human midbrain dopaminergic (DA) neurons (mDANs) from patients with a monoallelic SNCA locus duplication were differentiated from induced pluripotent stem cells (iPSC) and neuronal precursor cells (NPCs). Increased αSyn aggregation, increased levels of reactive oxygen species (ROS) in both cytoplasm and mitochondria (Mito.), mitochondrial dysfunction (measured by ATP levels), and increased neuronal cell death were determined in human iPSC-derived mDANs from patients with a monoallelic SNCA locus duplication, recapitulating neuropathological hallmarks of PD. Treatment of mDANs with the αSyn misfolding inhibitor NPT100-18A, ameliorating αSyn aggregation, specifically reduces mitochondrial ROS levels and rescues neuronal cell death in patient-derived neurons, thereby revealing the efficacy of the misfolding inhibitor in limiting loss of mDANs.

Supplementary Files

This is a list of supplementary files associated with this preprint. Click to download.

- SupplFigureS1.tif
- SupplFigureS2.tif
- SupplTableS1.docx